Predicting the evolutionary dynamic behavior of a laser with injected signal using Lyapunov exponents

D. K. Bandy, J. R. Hall, and M. E. Denker
Department of Physics, Oklahoma State University, Stillwater, Oklahoma 74078, USA
(Received 16 December 2014; published 23 July 2015)

We show that the role of the Lyapunov exponents can be extended beyond the customary local instability, such as limit cycle behavior, to include its use as an evolutionary predictor of the dynamics of a laser with injected signal (LIS). Numerical studies of LIS reveal that as a function of the input-signal strength the evolution of two nonzero Lyapunov exponents (generally equal) distinctively predicts the evolutionary trend of the fundamental frequency of the laser output signal (an important dynamic characteristic of the LIS) even with the presence of some noise. This globally predictive behavior of the Lyapunov exponents includes also the dynamic behavior of the individual coexisting attractors. Different coexisting attractors of LIS and configurations of Lyapunov exponents for both individual attractors and the global system are reported. Two LIS case studies are considered: (I) a high-gain system with a rich history of nonlinear behavior but not experimentally accessible, and (II) a low-gain system that has complex dynamics and is experimentally accessible for Class B lasers. Universality arguments support the thesis that these different configurations and the extended role of the Lyapunov exponents as an evolutionary predictor of the dynamics will be observed in other nonlinear, dynamic dissipative systems as well.

DOI: 10.1103/PhysRevA.92.013841 PACS number(s): 42.60.Mi, 05.45.Pq

I. INTRODUCTION

A unified description of cooperative behavior of multicomponent, nonlinear dynamical systems in chemistry, physics, biology, and engineering has universal appeal because of the widespread similarity of phenomena observed in these seemingly unrelated disciplines. Each structure or behavior has been cataloged and carefully compared for broad stability changes [1]. In the late 1960s nonlinear optical effects in passive driven systems emerged as one of the more interesting examples of cooperative behavior driven far from thermal equilibrium. It became known generally as optical bistability (OB) because it characterizes both the system and the phenomena. Seidel [2] first proposed an optical bistable scheme as a natural extension of his work in the microwave region. His patent reflects the excitement of the time and the potentially rich engineering possibilities, ranging from all-optical computers to optical communications. His work was followed by McCall [3] and Gibbs *et al.* [4] who created a host of experimental and theoretical studies, yet it was Bonifacio and Lugiato [5,6] in 1976 who provided the elegant first-principle treatment of optical bistability illustrating the existence of cooperative behavior and revealing profound analogies to first-order phase transitions. Seminal experimental studies in optical bistability were reported by Orozco, Rosenberger, and Kimble and co-workers [7–9] between 1983 and 1989.

The laser with injected signal is the active counterpart to optical bistability. It is as dynamically rich as OB and offers its own distinguishable and interesting output oscillations as a function of the driving field [10]. Just like OB, the instabilities are self-induced within the system without the assistance of a pump or parameter modulation. For a variety of conditions that are not experimentally accessible, yet interesting from nonlinear effects, a laser with injected signal (LIS) shows complicated self-pulsing regimes, such as limit cycles, torus behavior, period-doubling episodes, and chaos [11]. Multiple coexisting attractors are present for significant domains of the input signal [12]. Coexisting attractors are uniquely categorized by their phase-space, power spectra, temporal-field dynamics, and their Poincaré sections [13].

Studies of LIS continue today because of the abundance of open questions related to this complex system [14,15]. Even in steady state, LIS systems are studied with newer and more sophisticated theories. A recent publication that uses a generalized steady-state *ab initio* laser theory with injected signal, known as I-SALT, is explored by Cerjan and Stone [16]. It relates to Class A and B lasers primarily in the regime of microlasers.

In this paper we examine Lyapunov exponents (E^L's) not just as a useful tool for determining stability or the true nature of certain limit cycle bifurcations, [17] but rather as a predictor of the global dynamic behavior of nonlinear systems. LIS is the nonlinear system of choice in this investigation, but we believe other nonlinear systems will bear out similar results. Numerical analyses show that as a function of the injected signal, the trend of two nonzero E^L's (usually equal) is a predictor of the evolution of the fundamental (governing) frequency of the governing dynamics. We show that the nonzero E^L's are in fact unique for individual attractors. In the process of our investigation different coexisting attractors and structural behaviors of the Lyapunov exponents for individual attractors on the global scale are revealed as well.

We focus on two LIS systems. Both exhibit interesting self-pulsing, period-doubling episodes, chaos, and coexisting attractors. Case I is considered to be the canonical case study because of the extensive reporting on this system [17]. It is a high-gain system that is dynamically interesting, but not experimentally accessible. Case II is a low-gain system consistent with experimentally accessible Class B lasers. It is explored less extensively than Case I; nevertheless interesting dynamical behavior is indicated even for early stages of investigation [13]. We apply the same generic theoretical tools to investigate the second system as the first.

II. MODEL DESCRIPTION AND GENERAL FEATURES OF THE DYNAMICS

The laser with injected signal is a model based on homogeneously broadened two-level atoms. The atoms and the cavity are tuned to one another at the atomic frequency so that when there is no external signal, the laser operates stably with a carrier frequency ω_a. When the external cw beam with frequency $\omega_0 \neq \omega_a$ is injected into the ring cavity, competition is immediately established between the driving field and the laser oscillator. At low input-signal levels beat patterns with frequencies close to $|\omega_a - \omega_0|$ appear because of a simple mixing of the two fields where the laser acts as the local oscillator. At very high external signal levels the laser is predicted to lock stably to the injected field and produce a constant output intensity, known as injection locking. Between these two limits complicated and strange nonlinear phenomena can appear. Depending on the system parameters there are still many unexplained dynamical events. For example, the output signal can display as many as three different incommensurate frequencies for exactly the same driving field just by initiating different initial conditions.

The model is described by the traditional single-mode Maxwell-Bloch equations:

$$\frac{\partial X}{\partial \tau} = -\tilde{\kappa}\left[\left(1 - i\frac{\Phi}{\tilde{\kappa}}\right)X - Y + 2CP\right], \tag{1a}$$

$$\frac{\partial P}{\partial \tau} = -(1 + i\tilde{\Delta})P + XD, \tag{1b}$$

$$\frac{\partial D}{\partial \tau} = -\tilde{\gamma}\left[\frac{1}{2}(XP^* + X^*) + D + 1\right], \tag{1c}$$

where Y and X are proportional to the incident and emitted field amplitudes (Y is real and positive for definiteness, X is complex) and P and D are the normalized complex polarization and population difference, respectively. The system parameters are as follows: the small-signal atomic gain C, the scaled cavity relaxation rate $\tilde{\kappa} = \frac{\kappa}{\gamma_\perp}$, the scaled population decay rate $\tilde{\gamma} = \frac{\gamma_\parallel}{\gamma_\perp}$, the scaled cavity mistuning parameter $\Phi = \frac{(\omega_0 - \omega_c)}{\gamma_\perp}$, and the scaled atomic detuning from the injected-signal carrier $\tilde{\Delta} = \frac{(\omega_a - \omega_0)}{\gamma_\perp}$. $\gamma_\perp$ is the homogeneous linewidth. We assume that ω_a is close to the cavity mode frequency ω_c and that the injected signal oscillates with a carrier frequency ω_0 that is different from ω_c. The time, $\tau = \gamma_\perp t$, is measured in units of $\gamma_\perp^{-1}$. Our model is schematically represented in Fig. 1.

In steady state the input and output amplitudes are related by the state equation

$$Y = |X|\left[\left(1 - \frac{2C}{1 + \tilde{\Delta}^2 + |X|^2}\right)^2 + \left(\frac{2C\tilde{\Delta}}{1 + \tilde{\Delta}^2 + |X|^2} - \frac{\Phi}{\tilde{\kappa}}\right)\right]^{1/2}, \tag{2}$$

which can be single or triple valued depending on the system parameters. Obviously, in OB the S-shaped or triple-valued curve provides immediate information about the potential for bistable operation [18]. In LIS extensive stability searches thus far have not revealed the existence of a full hysteresis loop where coexisting, stable steady states exists. There is at least one study where a stable segment of the lower branch of the hysteresis loop can coexist with a stable segment of the upper branch [12].

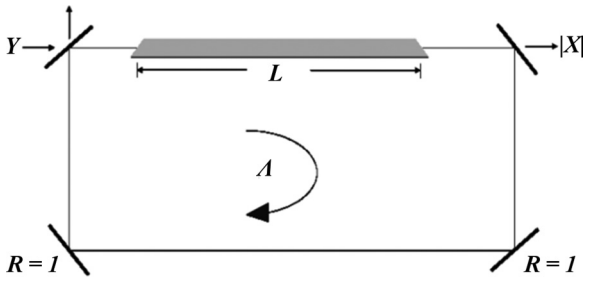

FIG. 1. Schematic representation of ring laser cavity with two partially transmitting mirrors and two perfectly reflecting mirrors. The length of the ring cavity is Λ, while the length of the active medium is L. Y and $|X|$ represent the scaled injected-field amplitude and the modulus of the output field, respectively.

A natural way to assess the various dynamical possibilities without the regimen of tools used in standard analyses is to assume a linear time dependence on the amplitude of the injected field. Even though LIS equations are no longer autonomous under this condition, imposing a slow ramp of the type $Y = Y_0 + v\tau$ on the injected signal gives qualitative results in the form of a time-dependent "sweep" that exposes the general dynamics of LIS. Empirical evidence from numerical data of both forward and backward sweeps shows that the output amplitude traces the stable segments of the state equation accurately; in addition, the pulsation patterns that are observed in the unstable domain (of the time-independent driving field) are reproduced with recognizable accuracy if the rate v of sweep is sufficiently small [12]. Evidence of coexisting attractors can be seen also. However, one must be careful because there is a lag effect in the dynamics. It occurs because the system is constantly having to adjust to a new and changing driving field; of course, the slower the sweep the less significant the lag.

Figure 2 is a graph of two steady-state curves for Cases I and II. Curve A corresponds to Case I and has control parameters $C = 20$, $\tilde{\Delta} = 1$, $\frac{\Phi}{\tilde{\kappa}} = -2$, $\tilde{\kappa} = 0.5$, and $\tilde{\gamma} = 0.05$, where the input field Y varies from 0 to about 25. Curve B corresponds to Case II and has control parameters $C = 3$,

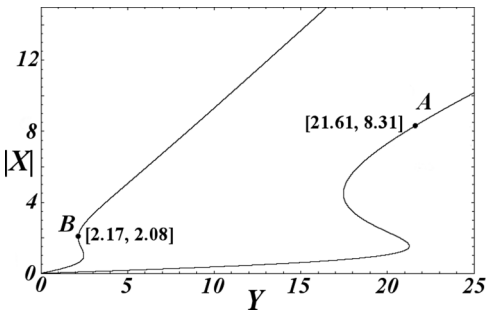

FIG. 2. Two state equations for a laser with injected signal corresponding to Case I marked A: $C = 20$, $\tilde{\Delta} = 1$, $\frac{\Phi}{\tilde{\kappa}} = -2$, $\tilde{\kappa} = 0.5$, and $\tilde{\gamma} = 0.05$; to Case II marked B: $C = 3$, $\tilde{\Delta} = 0.5$, $\frac{\Phi}{\tilde{\kappa}} = -0.5$, $\tilde{\kappa} = 0.1$, and $\tilde{\gamma} = 0.01$.

$\tilde{\Delta} = 0.5$, $\frac{\Phi}{\tilde{\kappa}} = -0.5$, $\tilde{\kappa} = 0.1$, and $\tilde{\gamma} = 0.01$, where Y varies from 0 to ~17. Both curves are triple valued and have a range of instability beginning at 0 and ending at the injection locking region labeled by their respective coordinates. The domain and range of each system is unambiguously different but as we shall show, the dynamics of these systems are similar.

One of the important tools that carried over from earlier studies of coexisting attractors is the so-called adiabatic scan [12]. The idea is, in essence, the same concept as defined in thermodynamics: Place the system in a specific state and change the control parameter ever so slightly so that the dynamics is disturbed only marginally as they evolve to a new state. For LIS we place the system inside the attractor by using as initial conditions the final stable-state values of a previous run and adjusting the Y value to be $Y + \delta Y$. We monitor the time evolution of the output amplitude to verify that the dynamics holds the attractor. This process of starting with known initial conditions for a specific attractor and holding it there for each small change in input signal allows the attractor to dynamically evolve and still hold its signature characteristics. The form of the attractor may change slightly but it remains distinguishable from other attractors that may coexist in the same Y domain.

III. HIGH-GAIN LIS: CASE I

Figure 3 represents a global view of the main dynamic features of the high-gain study. It is a schematic of the *relative position* of the fundamental frequency Ω_0 as a function of the injected-field amplitude Y over the domain of 0 to ~17. Ω_0 is identified in the power spectrum as the dominant frequency. Each spectrum characterizes a stable self-pulsing limit cycle of the attractor governed by the driving field. The up and down arrows indicate the approximate injected-signal transitions between attractors and the roman numerals I–VIII indicate the attractor number; $1P, 2P$, etc., represent the type of periodicity (QP is a type of torus) and $C1$, $C2$, and $C3$ represent the chaotic regions interrupted by domains of stable attractors. Details of the system's dynamics are explained in Ref. [13]. To indicate the additional interesting attractors found in the system, we label the positions of attractors VII and VIII (in red online) along with their global characteristic.

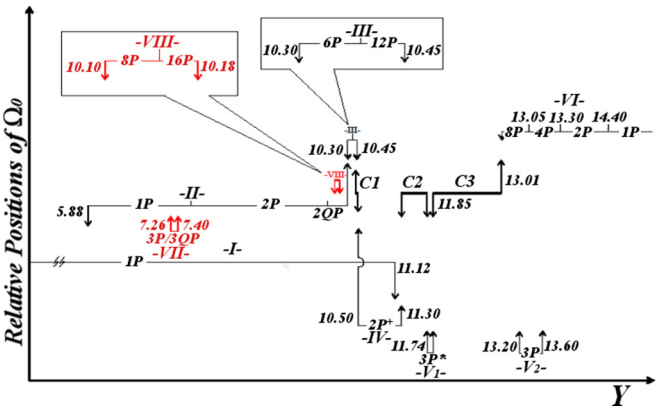

FIG. 3. (Color online) Schematic of the global behavior of the LIS system in which the relative portion of the fundamental frequency Ω_0 as a function of the injected-field amplitude over a domain of $5 < Y < 15$ is represented. The parameters are consistent with Case I. $1P$ denotes a singly periodic signal while $2P$, $3P$, $6P$, and $12P$ denote limit cycles with subharmonics of the fundamental $\Omega_0/2$, $\Omega_0/3$, $\Omega_0/6$, and $\Omega_0/12$, respectively; $2QP$ denotes quasiperiodic motion with two incommensurate frequencies (two-dimensional torus); $2P^+$ denotes an inverse Feigenbaum cascade; $3P^*$ denotes an inverse period-doubling sequence of the type 3×2^n; I–VIII represents attractors of the system; V_1 and V_2 are the different parts of attractor V; $C1$, $C2$, and $C3$ represent chaotic regions; the numbers, for example, 5.88, 11.12, etc., represent approximate threshold of transitions. Attractors VII and VIII in red are attractors identified in this study.

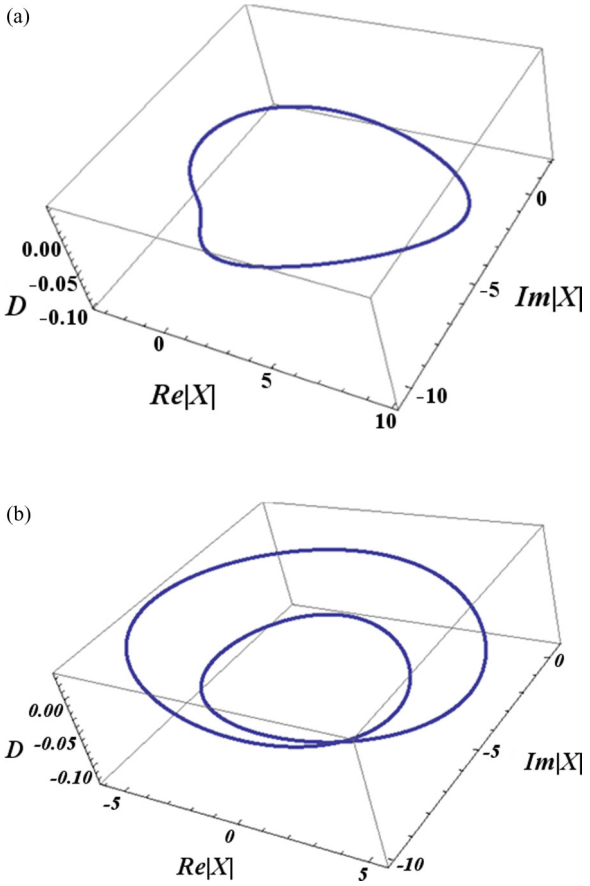

FIG. 4. (Color online) 3D phase-space plots for Case I with $Y = 9.6$ of (a) attractor I and (b) attractor II.

Figures 4 and 5 are samples of the dynamics of coexisting attractors I and II identified in the schematic of Fig. 3. They are distinctively different even though their dynamics are driven by the same value of the injected field. Figure 4 shows three-dimensional (3D) phase-space plots of the real and imaginary values of the output field and the population difference (Re$|X|$, Im$|X|$, D). Figure 5 shows the time-dependent dynamic behavior of the output amplitude $|X|$ as a function of time.

Another tool of analysis is the power spectrum generated by the Fourier spectral analysis of the output signal. Depending on the system parameters, the initial conditions of the dynamics, and the value of the injected signal, the spectrum of a limit cycle contains, at a minimum, a fundamental frequency and usually some combination of harmonics, subharmonics, beat

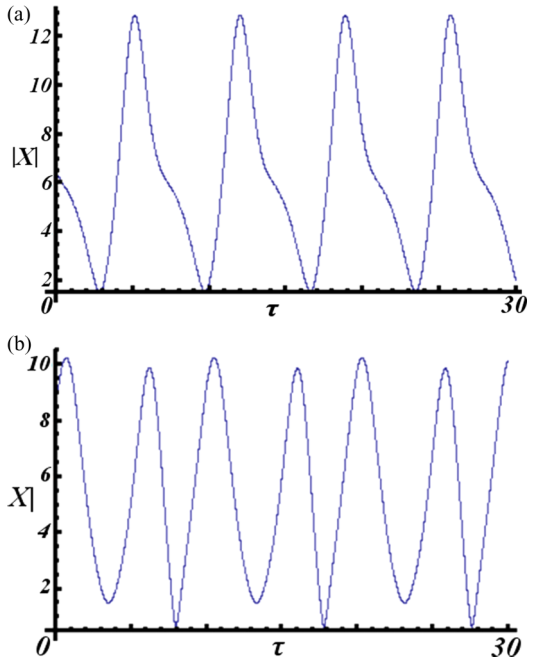

FIG. 5. (Color online) Case I output-field amplitude $|X|$ as a function of dimensionless time τ for $Y = 9.6$: (a) attractor I and (b) attractor II.

frequencies, and maybe sideband frequencies. If the spectrum is broadband with no real distinguishable frequencies, the spectrum identifies a chaotic output signal.

Figure 6 is the composite graph of the fundamental frequency Ω_0 of the temporal dynamics for Case I as a function of the input-field amplitude Y. It is created from power spectra of adiabatic scans of individual attractors. The domain of the fundamental frequencies of attractors VII and VIII are included, in addition to the previously known attractors (I –VI). [13]

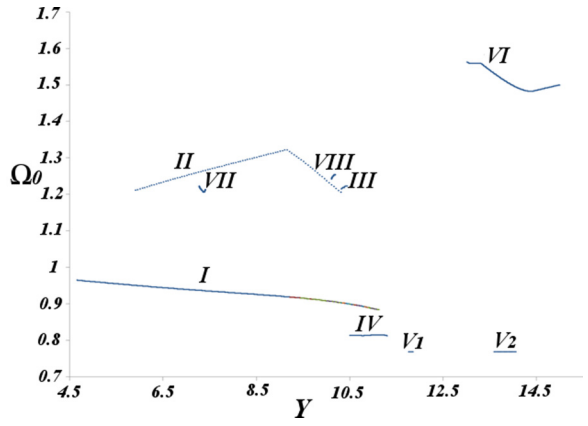

FIG. 6. (Color online) Behavior of the fundamental frequency Ω_0 generated from the Fourier transform of a given time-dependent trajectory as a function of the driving-field strength Y for parameters of Case I. I–VIII are the known attractors that evolve under the influence of distinct domains of attraction. Refer to Fig. 3 for the specific characteristics of these attractors. Open space denotes broadband behavior in the power spectrum where chaos is identified.

One might assume that Ω_0 should increase as the injected signal is increased; however, it is more complicated. In general, for a particular attractor and as a function of the injected signal we can demonstrate that where significant changes occur in the dominant frequency there occurs also a change in a specific dynamic event. We focus on attractors I, II, and VI of Fig. 6 as examples. In attractor I Ω_0 decreases simultaneously as the number of harmonic components in the power spectra increases. No other event occurs in the domain where attractor I exists. The dynamics of the output signal evolves remarkably uneventfully in phase space from the signature circular structure to a roughly oval pattern with a kink [Fig. 4(a)].

For attractor II and VI of Fig. 6, Ω_0 can both increase and decrease as a function of the injected signal, but not necessarily in that order. In the domain of attractor II a single event occurs in the dynamics that causes the increasing output frequency to change to decreasing output frequency. The single significant event is at $Y \approx 9$ where bifurcation of the output signal happens and the subharmonic appears in the spectra. The dynamics evolves as a period-doubling episode as expected. For attractor VI the dynamic signature is an inverse Feigenbaum sequence. In this attractor the disappearance of subharmonics and increasing appearance of harmonics and beat frequencies cause a decrease in the dominant frequency. At $Y \approx 14$ the event of the attractor completes its sequencing to a single oscillating limit cycle. At this point Ω_0 begins to increase in magnitude until injection locking where the attractor collapses to a fixed point. It should be noted that, on occasion, following the evolution of the dominant frequency Ω_0 can be risky especially when subharmonics appear in the spectra. The dominance of individual frequencies in this case can change and disguise the true dynamics. Getting the correct number of representative points for a given period of the motion is usually the culprit for this manifestation. Fourier transform programs are not always adequate at discriminating the dynamics as a whole and must be carefully monitored when plotting fundamental frequencies.

The set of spectral analyses builds the comprehensive frequency domain for self-pulsing LIS dynamics; however, an even more refined tool is the calculation of Lyapunov exponents. By definition Lyapunov exponents are quantities that characterize the rate of separation of infinitesimally close trajectories of dynamic systems. In general it is recognized that Lyapunov exponents E^L's provide a sensitive probe for the identification of bifurcation thresholds and bifurcated trajectories.

We begin our study of Lyapunov exponents by distinguishing between the global Lyapunov exponents and specific attractor Lyapunov exponents. In earlier work [17] the global dynamics of LIS was assumed to be the relevant dynamics for that particular injected-signal value under completely arbitrary start-up conditions or as an adiabatic scan of the entire domain of the injected signal without attractor consideration. Even though the uniqueness of coexisting attractors was known in 1985 their role in the global dynamics was not understood. The presumption at the time was that the attractors prevailed in the dynamics of LIS in some arbitrary way and that the global calculations of E^L's were in harmony with this behavior. Now it is clear that different coexisting

attractors can dominate under different circumstances over the same injected-field domain; the governance of the dominant attribution of individual attractors remains unknown to date. We use global characterization of Lyapunov exponents in light of this earlier work and we identify the attractors' Lyapunov exponents as unique to the individual attractors. Distinguishing the two is important in discussing the alternative global predictor characteristic of Lyapunov exponents.

While reproducing some of the dynamics of Case I we found different coexisting attractors, VII and VIII, for different domains of the input field. As stability condition (2)-(ii) of Ref. [17] suggests an attractor at $Y = 7.3$ might exist as a two-dimensional torus. Here the first two E^L's emerge as close to zero identifying the possible torus behavior. Unfortunately, that level of detail was not explored in 1985. In fact, searching for and finding a third coexisting attractor was not on the radar that close to the low end of the injected-field strength. Now we can report that is exactly the characteristic of attractor VII.

Attractor VII was discovered at $Y \approx 7.2634$ by serendipity. It coexists with attractors I and II and has a fundamental frequency that is incommensurate with the other two coexisting attractors. The magnitude of its fundamental frequency is located between the frequencies of the other two. Attractor VII is characterized as a $3P/3QP$ attractor because its trajectory at the onset is shown to be a period three and at the end a two-dimensional (2D) torus. Figures 7(a) and 7(b) show

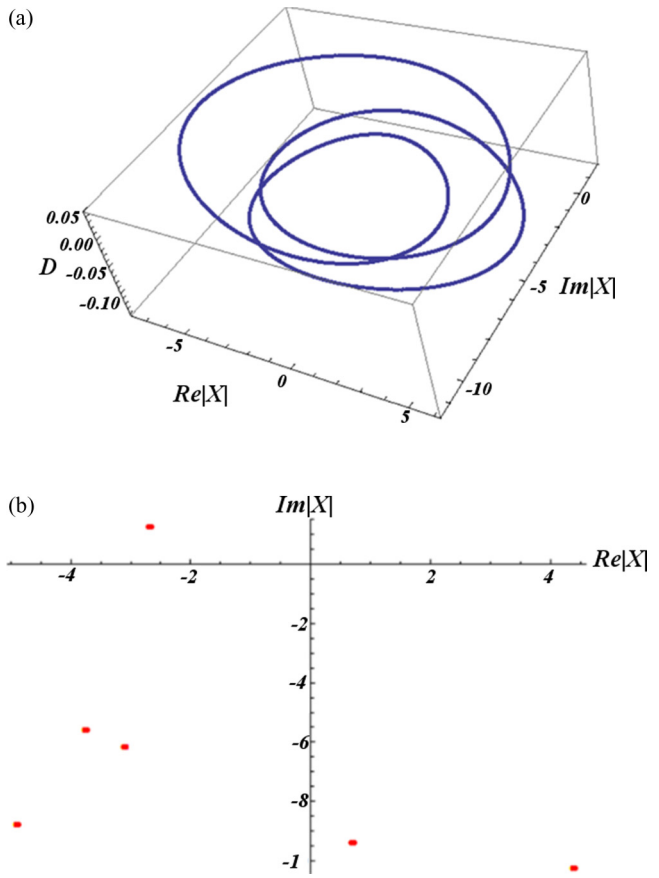

FIG. 7. (Color online) Parameters for Case I attractor VII for injected-field strength of $Y = 7.27$; (a) 3D phase-space plot; (b) 2D Poincaré surface of section.

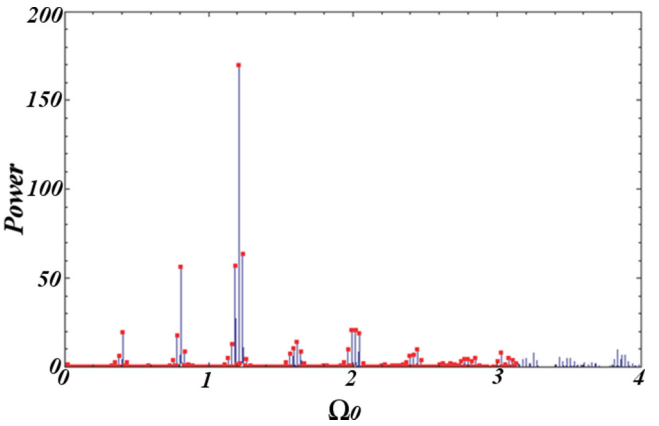

FIG. 8. (Color online) Power spectrum of torus dynamics for Case I and injected-field strength of $Y = 7.39$.

the $3P$ event in the 3D phase space and in the Poincaré section, respectively, at $Y = 7.27$; the Poincaré section is plotted with both the entry and exit points visible on the cross-sectional plane (in red online). At a slightly higher value of the injected signal $Y = 7.39$ attractor VII evolves into a 2D torus. The power spectrum in Fig. 8 not only shows the $\Omega_0/3$ subharmonic component, but also shows the sideband characteristic for torus behavior; the sideband frequency is $\sim$0.0258. The fundamental frequency is 1.2107, and the subharmonic $\Omega_0/3$ is 0.4036. Figures 9(a) and 9(b) are the temporal dynamics and the phase-space graph for $Y = 7.397$, respectively. Here

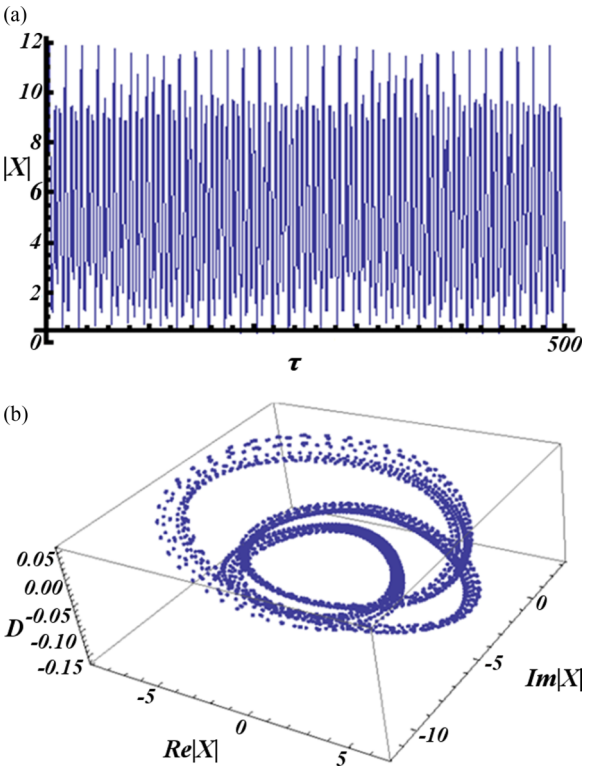

FIG. 9. (Color online) Case I parameters provide a temporal (a) and phase-space plot; (b) 3D of the torus behavior of attractor VII at an injected-signal strength of $Y = 7.397$.

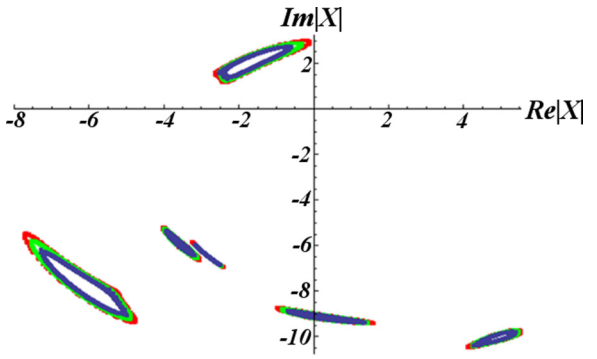

FIG. 10. (Color online) The evolution of the torus behavior of attractor VII with Case I parameters using a 2D Poincaré surface of section: red at $Y = 7.397$, green at $Y = 7.390$, and blue at $Y = 7.380$.

the expected "breathing" or sideband modulation is clearly demonstrated. Figure 10 is a 2D Poincaré section [analogous to Fig. 7(b)] showing the evolution of attractor VII for $Y = 7.38$, 7.39, and 7.397 (just before it collapses at $Y \approx 7.399\,92$), shown in red, green, and blue, respectively, online.

Attractor VIII is a narrow domain attractor that coexists with attractors I and II in the approximate region of $10.0981 < Y < 10.182$. Its fundamental frequencies (Ω_0's) are incommensurate with the frequencies of attractors I and II and are the largest of the three attractors. It is a region where complex dynamics might be expected because of its proximity to chaos; however, attractor VIII appears to be only an $8P/16P$ bifurcation structure. Our repeated attempts to establish a Feigenbaum sequence were never realized. As a result, we characterize this attractor as a limited $8P/16P$ attractor.

Other attractors have been found tentatively, but they are not revealed herein. For example, we believe there is an attractor located in the region previously characterized as a window (W) of periodicity $5PW$ [12]. In 1985 windows of periodicity were thought to be an intermittent behavior or window within chaos. Later studies argue that these windows are actually identifiable attractors [17]. This particular $5P$ region has some peculiar features that require further investigation before we make any attribution.

The most important development in the high-gain system is the strikingly similar behavior of the Ω_0's and the Lyapunov exponents during the adiabatic evolution of LIS as a function of injected signal. This similarity is especially vivid in the region of the second attractor. In Figs. 2 and 3 of Ref. [17] it is seen clearly that as a function of the injected signal the evolution of the Ω_0 corresponds qualitatively as the evolution of $E_4^L = E_5^L$. We reproduced these figures in Figs. 6 and 11, respectively, over the domain $Y \approx 4$–15. The scales of the ordinances of the E^L's and the Ω_0 in Fig. 11(b) are not the same so there are significant variations in the way they can be presented, but even in the most critical of presentations, their trends remain true as expected. The global E^L's of Eq. (1) are calculated while monitoring the 2D Poincaré surface of sections making sure the system is seated stably in its limit cycle for a given set of initial conditions.

Figures 11(a) and 11(b) show the first three and last two *globally* calculated E^L's of the dominant dynamics

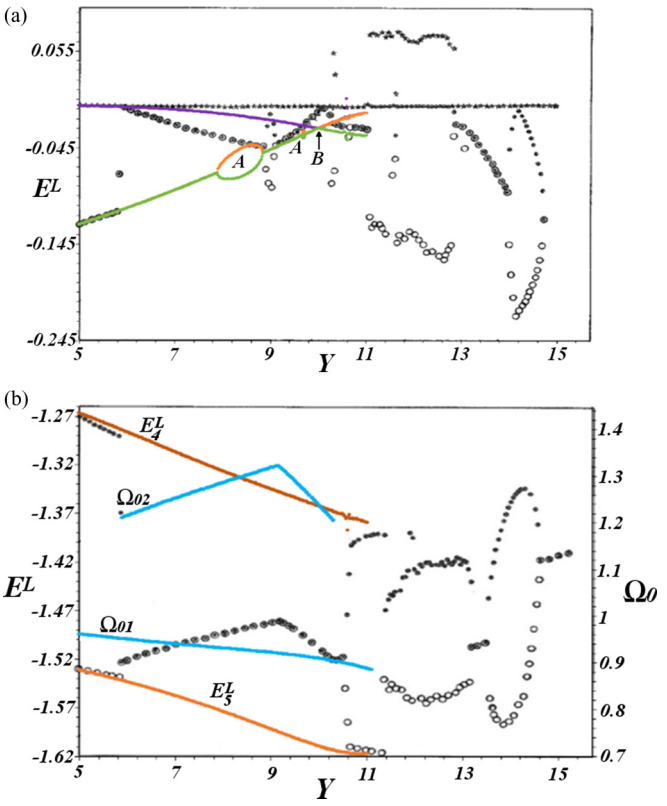

FIG. 11. (Color online) The Lyapunov exponents are shown for the global view in black and attractor I in colors. The fundamental frequencies Ω_0 of attractors I and II are shown overlaid on the original members as a function of the injected-field strength Y for Case I. Black circles with enclosed dots means that two equal E^L's are represented for a given value of Y [17]. (a) First three E^L's of attractor I are represented as solid lines in purple, orange, and green. Letter **A** marks E_2^L and E_3^L. (b) The Ω_0 of attractors I and II in blue are shown overlaid on the smallest two $E^L s$ marked E_4^L and E_5^L in brown for attractor I.

overlaid by the first three and last two E^L's of attractor I, respectively. In Fig. 11 our calculations of E^L's for attractor I are represented by solid lines and are distinguished from the global calculation represented as circles, dots, and stars. Two of the three nonzero E^L's of attractor I are marked with "**A**s" in Fig. 11(a) while in Fig. 11(b) the last two E^L's are shown marked with E_4^L and E_5^L. Some E^L's are equal in value and therefore overlay each other obscuring their individuality.

For example, in Fig. 11(a), within the region $Y \approx 5$–8 attractor I E^L's are shown attached to the global E^L's plotted as circles with enclosed dots. That is, $E_2^L = E_3^L$ for attractor I joins with the global $E_2^L = E_3^L$ as solid lines exposing clear differences in E^L's for coexisting attractors I and II. Attractor I E^L's are color coded orange and green online.

When plotting E^L's on the level of individual attractors, bubblelike structures can appear mirroring those observed on the global scale as a function of the injected field. In Fig. 11(a) it is E_2^L and E_3^L of attractor I that form the intermittent bubbles. At a value of $Y > 8$ where initially $E_2^L = E_3^L$, these Lyapunov exponents diverge simultaneously over a given domain of the injected signal and then converge back to their respective equal values; this cycle is repeated. The letter **A** marks the positions

of the bubbles. Notably one bubble is larger than the other. In the domains of these bubble structures, E_1^L, E_4^L, and E_5^L remain singular and unique.

The similarity in attractor I bubbles and in the distorted global bubble structures is impressive. In Figs. 11(a) and 11(b) we observe divergence and convergence in both $E_2^L = E_3^L$ and $E_4^L = E_5^L$, respectively. To what end this bubble structure indicates information about the system is not evident; it may, however, be a form of self-similarity. We do have clues, however. For example, on the global scale preliminary evidence indicates that the region between the global bubbles of the Lyapunov exponents, where two E^L's are equal, could designate the existence of a dominant attractor as in the case of attractor IV. Another unfamiliar occurrence appears in the structure of the Lyapunov exponents for an individual attractor. We observe that individual Lyapunov exponents align with or concatenate to trajectories of other Lyapunov exponents as a function of the injected field. For example, in attractor I in Fig. 11(a) we observe that E_3^L (in green online) concatenates to the end of E_2^L (in purple online) about midway between $Y = 9$ and $Y = 10$. This juncture is indicated with the letter **B** in Fig. 11(a).

Figure 11(b) shows the evolution of the fundamental frequency of attractors I and II marked as Ω_{01} and Ω_{02}, respectively (in blue online). These frequencies are overlaid in the graph of the global E^L's along with E_4^L and E_5^L of attractor I. E^L's of attractor I are solid lines (in orange online) attached to open circles and dots. Beyond attractors I and II the Lyapunov exponents are displayed globally as a reference to the whole system dynamics. Figure 11(b) shows two characteristics: (1) The dynamics, reflected in the continuous evolution of the Ω_0's, are evolving qualitatively as two equal E^L's of attractor I and II, respectively. Specifically Ω_{01} trends as both E_4^L and E_5^L ($E_4^L \neq E_5^L$) of attractor I and Ω_{02} trends as both E_4^L and E_5^L ($E_4^L = E_5^L$) of attractor II. (2) The *Y position where change occurs* in the dynamic event of attractor II is exactly the same *as the positional change* of the two smallest (and equal) E^L's. Attractor II dominants attractor I at about $Y \sim 7.3$ as evidenced in the forward sweep [Fig. 2(a) of Ref. [12]) while attractor II holds well past $Y \sim 7.3$ for deceasing Y until it collapses at $Y =\sim 5.88$. The latter condition is evident from the global E^L's behavior in Fig. 11(b).

Figures 12(a) and 12(b) show the dominant frequencies for attractors IV and VI marked as **AIV** and **AVI**, respectively, overlaid on the first three globally calculated E^L's. We note the scale is different for Ω_0. In Fig. 12(a) we show that the evolution of Ω_0's follow the trend of $E_2^L = E_3^L$ for attractor IV for the same domain of attraction. Similarly in Fig. 12(b), the general shape of the trajectory of Ω_0's taken in the domain of attractor VI is in good agreement with the general shape of two different sets of trajectories of E^L's. That is, when Ω_0 declines in value the trend follows $E_2^L = E_3^L$ as shown in Fig. 12(b) but as Ω_0 increases in value the trend follows $E_4^L = E_5^L$ [observable in Fig. 11(b)].

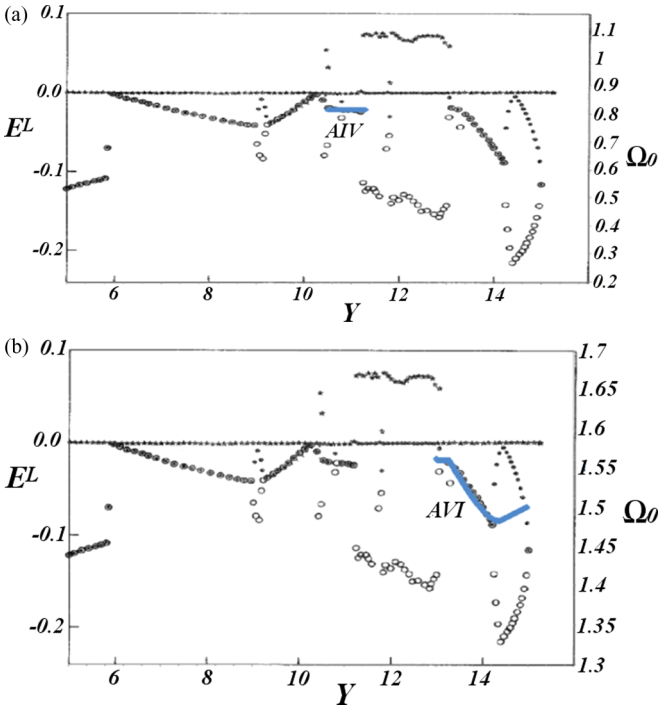

FIG. 12. (Color online) Global view of E^L's and the fundamental frequencies Ω_0 (in blue online) are shown overlaid as a function of the injected-field strength Y for Case I. (a) Ω_0 of attractor IV overlay the first three E^L's of the global view, marked AIV. (b) Ω_0 of attractor VI overlaid on the first three E^L's of the global view, marked with AVI.

IV. LOW-GAIN LIS: CASE II

The second system under investigation is the low-gain LIS system where the parameters are chosen for Class B lasers consistent with CO_2 lasers. It should be noted that unlike OB, where reducing the bistability parameter to experimentally accessible values causes the disappearance of higher-order bifurcations, it is opposite for LIS in experimental regimes. In fact, sweep dynamics reported in Fig. 13 of Ref. [12] indicate that different dynamics are possible under Case II experimental conditions. The forward and backward sweeps show that near the injection locking region there is a possibility for two coexisting attractors. Further studies that are shown in Fig. 5 of Ref. [12] confirm the distinctive temporal dynamics between the coexisting attractors.

Figure 13 shows the global view of the E^L's as a function of the injected field for Case II. Specifically, Fig. 13 shows the forward (in blue online) and backward (in red online) *adiabatic* scans of E^L's. The first three E^L's are shown in Fig. 13(a); the last two E^L's are shown in Fig. 13(b). The five individual E^L's are not color distinguished because we highlight three global features: (1) The global E^L's retrace identical paths whether in a forward or backward *adiabatic* scan with only a few exceptions. This portends that one attractor appears to be controlling most of the global dynamics. Bubblelike structures and some independent unidentified phenomena associated with the Lyapunov exponents are visible in Fig. 13(a). Bubbles are not present in Fig. 13(b), but there are some independent phenomena present. (2) There is at least one significant domain of the injected field where the Lyapunov exponents are not the same and the second attractor coexists. The coexisting attractors, which are not labeled for now, share the common

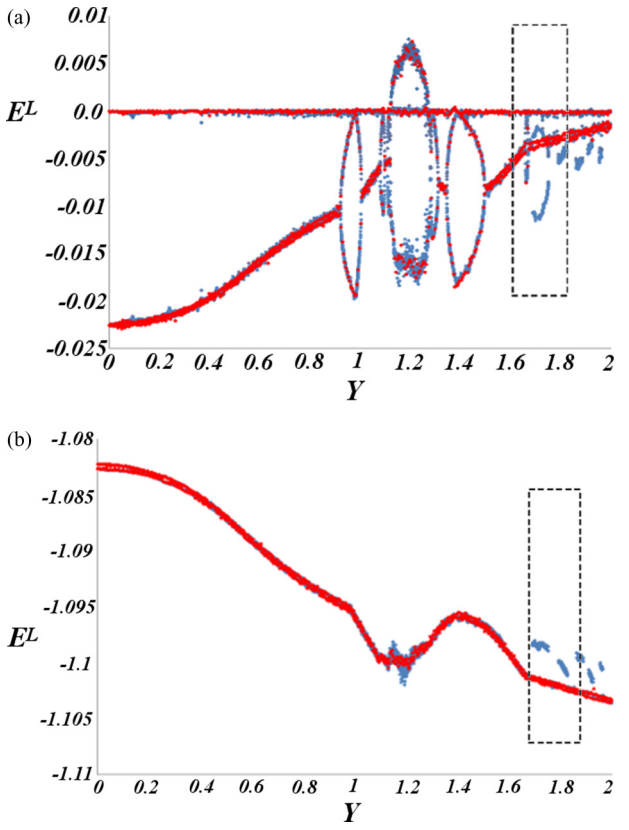

FIG. 13. (Color online) Global view for Case II of the Lyapunov exponents for the forward and backward adiabatic scans as a function of the injected-field strength Y. All five E^L's are in blue for the forward scan and in red for the backward scan; (a) the first three E^L's and (b) the last two E^L's.

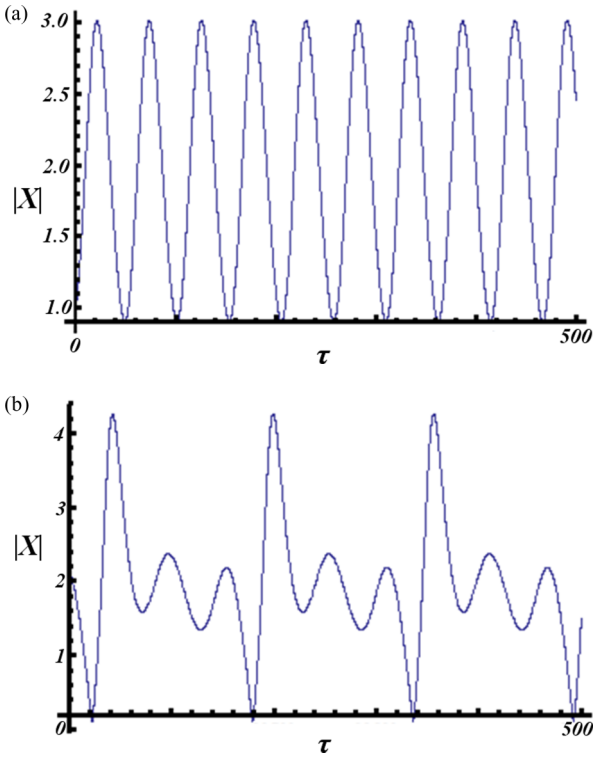

FIG. 14. (Color online) Output-field amplitude $|X|$ as a function of dimensionless time τ for parameters of Case II for $Y = 1.801$: (a) attractor I and (b) attractor II.

domain of about $1.6 < Y < 1.81$, a region distinguished by a dashed rectangle. (3) There is a region of chaos where the first Lyapunov exponent becomes positive, albeit with very small values.

Using the theoretical tools mentioned in Sec. I, we can report some characteristics of the coexisting attractors. For an injected-signal strength $Y = 1.801$ located close to the end of the domain of coexistence we show in Fig. 14 the time-dependent trajectories of the modulus of the field as a function of time. Clearly the output signals are different.

In Fig. 15 we show the different 3D phase-space plots of the coexisting attractors for the same injected-field strength as in Fig. 14. Figure 15(a) shows that one of the attractors is almost sinusoidal in structure while Fig. 15(b) shows the other is complicated and irregular. The Fourier analysis indicates interesting fundamental frequencies associated with these attractors.

Expanding on the global adiabatic scans of Fig. 13 we show Fig. 16, which includes the overlaid Ω_0's of the power spectra of both the global dynamics Ω_0 and the coexisting attractors Ω_{01} and Ω_{02}, respectively (in blue online). The five Lyapunov exponents for the attractors are enclosed in the dashed rectangle and one attractor is color coded for online.

Figure 16(a) shows the global E^L's overlaid with the Ω_0's as a function of the injected signal. The global Ω_0 is graphed as a solid line in the positive quadrant with its own ordinance. In general, the global evolution of the fundamental frequency follows the trend of two E^L's and likewise, the evolution of the attractor frequencies in the domain of coexistence follows the trend of two E^L's. Specifically, in the domain $0 < Y < 1$ the global Ω_0 increases and follows the trend of the trajectory of $E_2^L = E_3^L$.

There are three other nonchaotic domains of the injected signal, (1) $1.0 < Y < 1.11$, (2) $1.275 < Y < 1.59$, and (3) $1.605 < Y < 2.17$, where the trend of E^L's predicts the dynamics of this laser system. Namely, the evolution of Ω_0 in regions (1) and (2) are consistent with the trend of the two Lyapunov exponents $E_4^L = E_5^L$ shown in Fig. 16(b). The evolution of Ω_0 in region (3) follows the trend of the two Lyapunov exponents $E_2^L = E_3^L$ shown in Fig. 16(a). In the last region (3) there appears to be a choice in two sets of equal E^L's to follow. Upon further inspection, however, this is the region just before injection locking and there are no significant dynamic events to alter the increase in the output signal. So the logical choice is the set $E_2^L = E_3^L$. Between regions (2) and (3) is the region of chaos.

V. SUMMARY AND DISCUSSION

It is true that research on nonlinear dynamics including the role of Lyapunov exponents has been extensively explored since 1980 [1]. Cutting-edge investigators understood and reported on the many relationships connecting Lyapunov exponents (E^L's) to dynamic features of nonlinear systems such as steady states, limit cycles, torus behavior, or chaos. However, the hypothesis that E^L's had an evolutionary

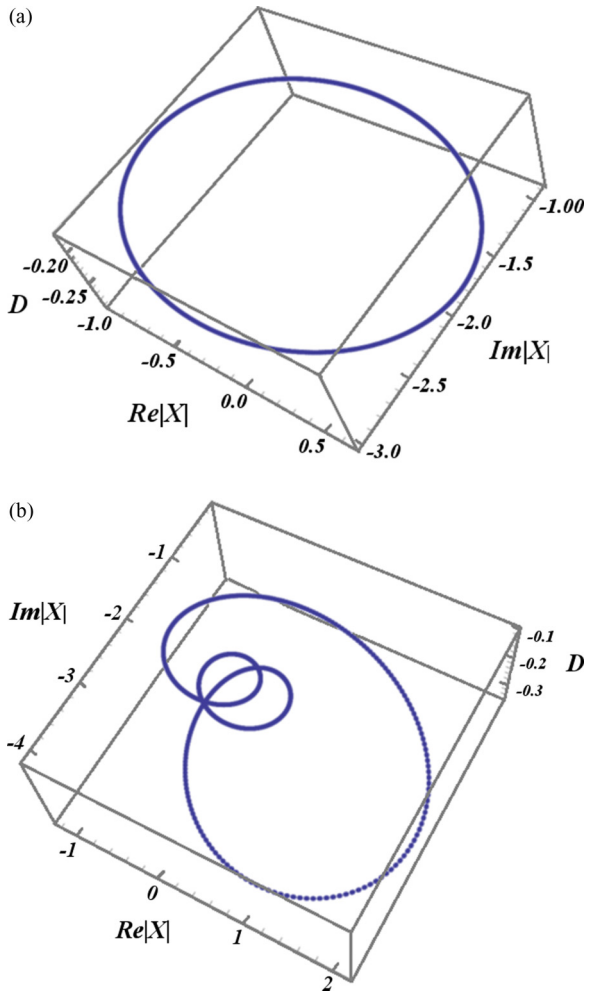

FIG. 15. (Color online) 3D phase-space plots of (a) attractor I and (b) attractor II for Case II with $Y = 1.801$.

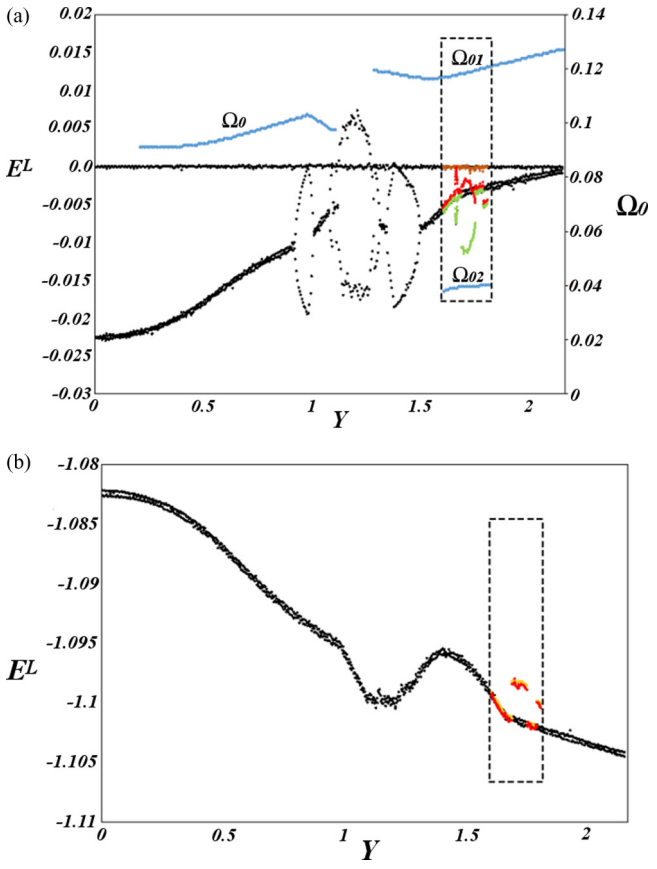

FIG. 16. (Color online) Case II global view of E^L's for a backward adiabatic scan as a function of the injected field Y. The coexistence domain is identified by a dashed rectangle: (a) the first three E^L's and Ω_0, Ω_{01}, and Ω_{02}; (b) the last two E^L's.

predictive aspect to their calculations was illusive; no one saw E^L's as a predictor of the *global dynamics of the nonlinear system as a whole.*

In this paper we show that the role of the Lyapunov exponents can be extended beyond the customary stability considerations to include its use as a predictor of the global dynamics of nonlinear systems. We use the laser with injected signal as the investigative nonlinear system. Numerical studies of LIS reveal that as a function of the input signal the evolution of two nonzero Lyapunov exponents (generally equal) predicts the evolution of the fundamental frequency of the output signal, an important dynamic characteristic of the LIS. This predictive behavior of the Lyapunov exponents includes also the dynamic behavior of the individual coexisting attractors. Alternative coexisting attractors of LIS and configurations of Lyapunov exponents for both individual attractors and the global system are examined. Two LIS case studies are considered: (I) a high-gain system with a rich history of nonlinear behavior but not experimentally accessible, and (II) a low-gain system that has complex dynamics and is experimentally accessible for Class B lasers. Universality arguments support the thesis that these unique structures and the extended role of the Lyapunov exponents as a predictor of dynamic evolution will be observed in other nonlinear, dynamic, dissipative systems as well.

The E^L's are a set of simple numbers that reflect the rate of separation of infinitesimally close trajectories and are calculated as a result of computational noise. They are in essence an m-dimensional volume contracting or expanding depending on system parameters (m is an integer). The sum of these E^L's is functionally dependent on the decay rates that govern the dynamics of the nonlinear model. The sum of E^L's *remains constant* regardless of a change in the control parameter. Fundamentally, this sum is represented by the $\mathrm{Tr}[\hat{J}]$ where $\hat{J}$ is the linear matrix of the governing system. For Case I the sum of E^L's is 3.05 and for Case II the sum of E^L's is 2.01. As the control parameter changes, E^L's *rearrange* themselves in such a way as to *predict* the trend of the evolution of the full-blown *nonlinear* governing system (all the while their sum remains steadfast). It is fascinating that these simple numbers can portend the evolution of the fully developed nonlinear dynamic system.

We support the main hypothesis of this paper using LIS dynamics. However, during the investigation intriguing features of E^L's associated with individual attractors and global features of LIS were also observed. They can be summarized in the following discussion.

The two supporting LIS Cases I and II that are reported herein are different mainly because one is experimental and the other is not. However, they both have interesting nonlinear behaviors: (1) They experience period doubling, chaos, and coexisting attractors. (2) They have two nonzero Lyapunov exponents calculated as a function of the injected-field strength that predict the evolution of the dynamics of LIS when monitoring the dominant frequency of the power spectrum of the output signal. (3) They support bubble structures in the evolution of the Lyapunov exponents as a function of the injected field on both the global and attractor scale.

These three nonlinear behaviors are shown in specific circumstances. The evolution of the fundamental frequencies in the dynamics compares favorably to the trend of $E_2^L = E_3^L$ or $E_4^L = E_5^L$ or even $E_4^L \neq E_5^L$ given the conditions of the system. Further, as a function of the injected field we find that two E^L's initially identical in a single attractor can diverge and then converge back to a single value simultaneously forming a bubblelike structure. This event is repeated usually at least once. These structures are experienced on the global scale as distorted bubbles in E_2^L and E_3^L, and E_4^L and E_5^L; as a finer detail, the global bubbles are often found separated by regions of $E_2^L = E_3^L$ and $E_4^L = E_5^L$, respectively. Preliminary evidence indicates importantly that this equality region may herald the existence of an attractor that may coexist with others in the system.

We report for the high-gain case that within a given attractor, E^L's of one ilk can concatenate to the trajectory of another as a function of the injected field. The location of this concatenation does not appear to predict any obvious shift in dynamic trends, but it is premature to forecast. Also we report two interesting attractors in Case I that coexist with attractors I and II. One attractor has dynamics that includes stable two-torus behavior that collapses as the input signal changes to another stable coexisting attractor—not to chaos. The other attractor has a small Y domain and is limited in its bifurcation sequence. Can these attractors be accessed experimentally?

The effects of noise on these findings broadens the scope of this study beyond the confines of the paper; however, we believe it is worthy of some brief comments.

For both Cases I and II the model includes an injected signal that is represented arguably simplistically as an amplitude and frequency. In reality the injected signal can have fluctuations that we designate as noise in the form of either (1) a slow-frequency drift of the injected signal, or (2) a fast-frequency jitter that manifests itself as the linewidth of the laser signal. We use a random number generator scaled appropriately and with different strengths to explore these two forms of noise. Our preliminary results involve the two outlying regions: (1) where the injected signal is weak at the beginning of the unstable steady-state region, and (2) where the injected signal is strong at the end of the unstable region and just before the stable steady state. Between these two regions the dynamics is complicated and chaotic.

For Case II in the form of slow noise, we find that for both outlying regions studied, (1) the fundamental frequencies of the noisy power spectra plot as a scatter plot around the model's fundamental frequencies without noise (Fig. 16), as expected. A linear fit of the noisy frequencies follows the linear trend of the E^L's with reasonable accuracy just as the model frequencies do when there is no noise. (2) We find that there is opportunity for both attractors in the coexisting region to be accessed depending on the strength of the noise.

For Case II in the form of fast noise, the results are so disparate that we can only say the studies are ongoing.

It takes only a brief excursion into noise to conclude that modeling noise can be an important tool to understanding noisy experimental systems, but also we may find that noise can give us guidance into understanding how the attractors are accessed or even into why one attractor dominates another. The potential for observing two different output frequencies (maybe not three) for the same physical setup is a worthy experiment that is achievable for the parameters of Case II. Experimental confirmation of different coexisting attractors in LIS would be very interesting.

Finally, the evolutionary dynamic predictive behavior of the Lyapunov exponents holds even with the introduction of some noise.

ACKNOWLEDGMENTS

We thank Al Rosenberger for his helpful discussions. We are grateful to undergraduates Aaron Braly and Erikk Burton for their valuable computations and useful interactions.

[1] See, for example, J. Guckenheimer and P. Holmes, *Nonlinear Oscillations, Dynamical Systems, and Bifurcations of Vector Fields* (Springer-Verlag, New York, 1983); H. Haken, *Synergetics: An Introduction* (Springer-Verlag, New York, 1983); H. G. Schuster and W. Just, *Deterministic Chaos: An Introduction, Fourth Edition* (Wiley-VCH, Berlin, 2005); L. M. Narducci and N. B. Abraham, *Laser Physics and Laser Instabilities* (World Scientific, Singapore, 1980).

[2] H. Seidel, U.S. Patent No. 3610-731 (1971).

[3] S. L. McCall, Phys. Rev. A **9**, 1515 (1974).

[4] H. M. Gibbs, S. L. McCall, and T. N. C. Venkatesan, Phys. Rev. Lett. **36**, 113 (1976).

[5] R. Bonifacio and L. A. Lugiato, Opt. Commun. **19**, 172 (1976).

[6] R. Bonifacio and L. A. Lugiato, Lett. Nuovo Cim. **21**, 517 (1978).

[7] L. A. Orozco, A. T. Rosenberger, and H. J. Kimble, Phys. Rev. Lett. **53**, 2547 (1984).

[8] L. A. Orozco, A. T. Rosenberger, and H. J. Kimble, Phys. Rev. A **36**, 3248 (1987).

[9] L. A. Orozco, H. J. Kimble, A. T. Rosenberger, L. A. Lugiato, M. L. Asquini, M. Brambilla, and L. M. Narducci, Phys. Rev. A **39**, 1235 (1989).

[10] H. Haken, *Light: Laser Dynamics* (North-Holland Physics, New York, 1985), Vol. 2.

[11] L. A. Lugiato, L. M. Narducci, D. K. Bandy, and C. A. Pennise, Opt. Commun. **46**, 64 (1983).

[12] D. K. Bandy, L. M. Narducci, and L. A. Lugiato, J. Opt. Soc. Am. **B2**, 148 (1985).
[13] D. J. Jones and D. K. Bandy, J. Opt. Soc. Am. **B7**, 2119 (1990).
[14] J. Ohtsubo, *Semiconductor Lasers: Stability, Instability, and Chaos* (Springer, New York, 2007).
[15] S. Wieczorek, B. Krauskopf, T. B. Simpson, and D. Lenstra, Phys. Rep. **416**, 1 (2005).
[16] A. Cerjan and A. D. Stone, Phys. Rev. A **90**, 013840 (2014).
[17] Y. Gu, D. K. Bandy, J-M Yuan, and L. M. Narducci, Phys. Rev. A **31**, 354 (1985).
[18] M. B. Spencer and W. E. Lamb, Jr., Phys. Rev. A **5**, 884 (1972).